Available online at www.sciencedirect.com
ScienceDirect
Journal of Computational Physics 226 (2007) 2341–2358
JOURNAL OF COMPUTATIONAL PHYSICS
www.elsevier.com/locate/jcp

A low-variance deviational simulation Monte Carlo for the Boltzmann equation

Thomas M.M. Homolle [a], Nicolas G. Hadjiconstantinou [b,*]

[a] *Aeronautics and Astronautics Department, Massachusetts Institute of Technology, Cambridge, MA 02139, United States*
[b] *Mechanical Engineering Department, Massachusetts Institute of Technology, Cambridge, MA 02139, United States*

Received 19 February 2007; received in revised form 12 July 2007; accepted 17 July 2007
Available online 27 July 2007

Abstract

We present an efficient particle method for solving the Boltzmann equation. The key ingredients of this work are the variance reduction ideas presented in Baker and Hadjiconstantinou [L.L. Baker, N.G. Hadjiconstantinou, Variance reduction for Monte Carlo solutions of the Boltzmann Equation, Physics of Fluids, 17 (2005) (art. no, 051703)] and a new collision integral formulation which allows the method to retain the algorithmic structure of direct simulation Monte Carlo (DSMC) and thus enjoy the numerous advantages associated with particle methods, such as a physically intuitive formulation, computational efficiency due to importance sampling, low memory usage (no discretization in velocity space), and the ability to naturally and accurately capture discontinuities in the distribution function. The variance reduction, achieved by simulating only the deviation from equilibrium, results in a significant computational efficiency advantage for low-signal flows (e.g. low flow speed) compared to traditional particle methods such as DSMC. In particular, the resulting method can capture arbitrarily small deviations from equilibrium at a computational cost that is independent of the magnitude of this deviation. The method is validated by comparing its predictions with DSMC solutions for spatially homogeneous and inhomogeneous problems.

Keywords: Boltzmann equation; Numerical solution; Particle method; Variance reduction; Nanoscale gas flow

1. Introduction

Interest in numerical solution of the Boltzmann equation [1,2] has recently been revived in connection with small-scale science and technology. In typical MEMS/NEMS applications, characteristic flow scales are no longer much larger than the molecular mean free path, requiring modeling beyond the Navier–Stokes level of description. Numerical solution of the Boltzmann equation for low-signal (e.g. low-speed) flows typical of this regime [18,19] remains a formidable task; this is due to the fact that the prevalent method for solving the Boltzmann equation, a stochastic particle simulation method known as the direct simulation Monte Carlo

* Corresponding author. Tel.: +1 617 452 2280; fax: +1 617 258 5802.
E-mail address: ngh@mit.edu (N.G. Hadjiconstantinou).

0021-9991/$ - see front matter
doi:10.1016/j.jcp.2007.07.006

(DSMC) [7], becomes very inefficient in low-signal flows due to the uncertainty associated with the statistical sampling of hydrodynamic properties from particle data. More specifically, it can be shown [10] that, at constant relative statistical uncertainty (a measure of signal to noise ratio), the computational cost of DSMC increases as Ma^{-2} for $Ma \to 0$, making noise-free simulation of low-speed, or more generally low-signal, flows very expensive and in some cases intractable.

Deterministic methods for solving the Boltzmann equation are typically very computationally expensive due to the high dimensionality of the distribution function in general and the additional high cost and storage requirements associated with the numerical treatment of the Boltzmann collision integral in particular. Moreover, in problems of practical interest, the existence of propagating discontinuities in the distribution function significantly reduces the number of viable approaches. Here we note the numerical solution method of Sone et al. [14] who, by carefully treating the discontinuities in the distribution function, were able to provide accurate solutions to a number of *spatially dependent*– albeit special[1]– problems of interest [14–16] on the basis of the linearized Boltzmann equation. Extensions of this approach to higher spatial dimensions have been limited to cases where the collision integral is replaced by the BGK collision model (e.g. see [17]).

In this paper we present an approach for solving the original Boltzmann equation using a Monte Carlo method which retains the various desirable features associated with DSMC while addressing the serious limitation suffered by Monte Carlo approaches in the limit of small deviation from equilibrium. The foundation for the present approach was laid in a previous Letter [3] where Baker and Hadjiconstantinou presented the general idea of variance reduction for Monte Carlo solutions of the Boltzmann equation. Specifically, it was shown in [3] that by simulating only the deviation from equilibrium, it is possible to construct Monte Carlo solution methods that can capture arbitrarily small magnitudes of this deviation at a computational cost that is independent of the latter. These features were demonstrated (in the same Letter) by applying the variance reduction technique to a finite volume formulation of the Boltzmann equation.

The new particle method presented here will be referred to as LVDSMC: low-variance deviational simulation Monte Carlo. As mentioned above, this method incorporates variance reduction while retaining the algorithmic structure and most basic features of DSMC. As discussed before [3], particle methods have a number of advantages which include simplicity, an intuitive formulation which naturally employs importance sampling, and very low memory usage. Moreover, their natural treatment of the advection process means that they can easily handle and accurately capture traveling discontinuities in the distribution function.

Finally we note that ideas similar in spirit, namely simulation of the deviation from a Maxwell–Boltzmann distribution to reduce the statistical uncertainty, have been used in the simulation of gyrokinetic equations [20,21]. We also remark that Fokker–Planck-inspired, "quiet" Monte Carlo particle simulation methods have been developed for solving the Euler system of equations [22] and the diffusion equation [23].

2. Boltzmann equation

Here we consider a hard-sphere [2] gas of molecular mass m and hard-sphere diameter d, at a reference temperature T_0 and reference number density n_0. The mean free path is given by $\lambda_0 = 1/(\sqrt{2}\pi n_0 d^2)$, the most probable molecular speed by $c_0 = \sqrt{2kT_0/m}$, and the molecular collision time by $\tau_0 = \sqrt{\pi}\lambda/(2c_0)$, respectively, where k is Boltzmann's constant. Let $f(\mathbf{r},\mathbf{c},t)$ be the velocity distribution function [2], where $\mathbf{r} = (x,y,z)$ is the position vector in physical space, $\mathbf{c} = (c_x,c_y,c_z)$ is the molecular velocity vector, and t is time. In this paper we limit our discussion to the case where no external fields are present; extension of this work to the presence of external fields is straightforward. In the absence of external fields, the Boltzmann equation can be written [2] in the following form:

$$\frac{\partial f}{\partial t} + \mathbf{c}\cdot\frac{\partial f}{\partial \mathbf{r}} = \left[\frac{\mathrm{d}f}{\mathrm{d}t}\right]_{\mathrm{coll}} (\mathbf{r},\mathbf{c},t) \tag{1}$$

with

[1] These problems are one-dimensional in space and such that similarity transformations reduce the problem dimensionality in velocity space to two, while discontinuities in the distribution function are stationary and can be easily aligned with mesh-element boundaries.

$$\left[\frac{\mathrm{d}f}{\mathrm{d}t}\right]_{\mathrm{coll}}(\mathbf{r},\mathbf{c},t)=\frac{1}{2}\int\int\int(\delta_2'+\delta_1'-\delta_2-\delta_1)f_1f_2g\sigma\,\mathrm{d}^2\Omega\,\mathrm{d}^3\mathbf{c}_1\,\mathrm{d}^3\mathbf{c}_2 \tag{2}$$

where $\sigma=d^2/4$ is the differential collision cross-section for hard spheres, $f_1=f(\mathbf{r},\mathbf{c}_1,t)$, $f_2=f(\mathbf{r},\mathbf{c}_2,t)$, $\delta_1=\delta^3(\mathbf{c}_1-\mathbf{c})$, $\delta_2=\delta^3(\mathbf{c}_2-\mathbf{c})$, $\delta_1'=\delta^3(\mathbf{c}_1'-\mathbf{c})$ and $\delta_2'=\delta^3(\mathbf{c}_2'-\mathbf{c})$. Here $\mathbf{c}_1$, $\mathbf{c}_2$ are the precollision velocities, $g=|\mathbf{c}_1-\mathbf{c}_2|$ is the magnitude of the relative velocity vector, and $\mathbf{c}_1',\mathbf{c}_2'$ are the postcollision velocities, related to the precollision velocities through the scattering angle Ω. Here, and in the remainder of the paper, integration in velocity space extends from $-\infty$ to ∞ unless otherwise stated; similarly, the solid angle integration is over the surface of the unit sphere, unless otherwise stated.

2.1. Particle methods for solving the Boltzmann equation

The most prevalent Boltzmann solution method is a particle method known as direct simulation Monte Carlo (DSMC). DSMC solves [9] the Boltzmann equation by simulating molecular motion as a series of timesteps, each of length Δt, and during which a collisionless advection and collision substep are performed [7]. This can be thought of as a splitting scheme in which the collisionless advection substep integrates

$$\frac{\partial f}{\partial t}+\mathbf{c}\cdot\frac{\partial f}{\partial \mathbf{r}}=0 \tag{3}$$

while the collision substep integrates

$$\frac{\partial f}{\partial t}=\left[\frac{\mathrm{d}f}{\mathrm{d}t}\right]_{\mathrm{coll}} \tag{4}$$

During the advection substep, the positions of all particles are updated according to their velocities, while the velocities remain constant. During the collision substep, the distribution function is updated by processing binary collisions between collision partners chosen at random within the same computational cell. The collision rules can be derived [3] from (2): collisions occur between pairs of particles (1 and 2) drawn from the underlying distribution (f_1 and f_2, respectively). The collision leads to the creation of 4 new particles: $\delta_1',\delta_2',-\delta_1,-\delta_2$. However, the newly created particles $-\delta_1$, $-\delta_2$ cancel the colliding particles and thus the algorithm simply proceeds by updating particles $1,2\rightarrow 1',2'$. DSMC owes much of its success to this formulation, which is not only simple and physically intuitive, but it also performs importance sampling, thus endowing it with formidable computational efficiency.

3. Variance reduction in particle methods

Given the long list of advantages enjoyed by particle methods, but also due to historical reasons, a particle method which incorporates variance reduction is highly desirable. In this section we discuss a basic particle scheme incorporating variance reduction as a means of elucidating the major challenges associated with variance reduction in particle schemes. Readers interested in pde-type solution methods incorporating variance reduction are referred to [3,13].

As shown [3] before, a variance-reduced formulation is obtained by considering the deviation $f^{\mathrm{d}}\equiv f-f^{\mathrm{MB}}$ from an *arbitrary* Maxwell–Boltzmann distribution,

$$f^{\mathrm{MB}}(\mathbf{c})=\frac{n_{\mathrm{MB}}}{\pi^{3/2}c_{\mathrm{MB}}^3}\exp\left[-\frac{(\mathbf{c}-\mathbf{u}_{\mathrm{MB}})^2}{c_{\mathrm{MB}}^2}\right] \tag{5}$$

In the work that follows this distribution will be identified with the local equilibrium distribution and thus $c_{\mathrm{MB}}=\sqrt{2kT_{\mathrm{MB}}/m}$ is the most probable speed based on the local equilibrium temperature T_{MB}, and $\mathbf{u}_{\mathrm{MB}}$ is the local equilibrium flow velocity. Upon substitution into Eq. (2), we obtain

$$\left[\frac{\mathrm{d}f}{\mathrm{d}t}\right]_{\mathrm{coll}}(\mathbf{r},\mathbf{c},t) = \left[\frac{\mathrm{d}f^{\mathrm{d}}}{\mathrm{d}t}\right]_{\mathrm{coll}}(\mathbf{r},\mathbf{c},t)$$
$$= \frac{1}{2}\int\int\int \left(\delta_2' + \delta_1' - \delta_2 - \delta_1\right)\left(f_1^{\mathrm{MB}} f_2^{\mathrm{d}} + f_2^{\mathrm{MB}} f_1^{\mathrm{d}} + f_1^{\mathrm{d}} f_2^{\mathrm{d}}\right) g\sigma\,\mathrm{d}^2\Omega\,\mathrm{d}^3\mathbf{c}_1\,\mathrm{d}^3\mathbf{c}_2$$
$$= \mathcal{L}^{\mathrm{MB}}(f^{\mathrm{d}}) + \mathcal{J}(f^{\mathrm{d}}, f^{\mathrm{d}}) \tag{6}$$

since the integral involving $f_1^{\mathrm{MB}} f_2^{\mathrm{MB}}$ is identically zero. The last equality shows that the collision integral can be written as the sum of a linear $[\mathcal{L}^{\mathrm{MB}}(f^{\mathrm{d}})]$ and a quadratic $[\mathcal{J}(f^{\mathrm{d}}, f^{\mathrm{d}})]$ term. Separating terms and using the fact that the linear terms are symmetric with respect to interchanging $\mathbf{c}_1$ and $\mathbf{c}_2$ gives

$$\left[\frac{\mathrm{d}f}{\mathrm{d}t}\right]_{\mathrm{coll}}(\mathbf{r},\mathbf{c},t) = \frac{1}{2}\int\int\int \left(\delta_2' + \delta_1' - \delta_2 - \delta_1\right) f_1^{\mathrm{d}}\left(2f_2^{\mathrm{MB}} + f_2^{\mathrm{d}}\right) g\sigma\,\mathrm{d}^2\Omega\,\mathrm{d}^3\mathbf{c}_1\,\mathrm{d}^3\mathbf{c}_2 \tag{7}$$

We thus seek to develop a particle formulation in which particles simulate the deviation from equilibrium f^{MB}. Collision rules for the deviational particles are to be *rigorously* derived from the "new", variance-reduced collision integral (Eq. (7)). Particles may be positive or negative, depending on the sign of the deviation from equilibrium at the location in phase space where the particle resides. As in DSMC, each *computational* deviational particle represents an *effective number* of physical deviational particles, denoted as N_{eff}. In the present implementation, the effective number is common for all particles.

Based on our choice for the underlying equilibrium distribution, f^{MB}, the advection substep may be different [5,6,8] from DSMC. We will discuss the advection substep in Section 4.2, when our choice for the underlying equilibrium distribution f^{MB} has been explained.

The first attempt towards deriving the new collision rules may proceed by writing (7) in the following form

$$\left[\frac{\mathrm{d}f}{\mathrm{d}t}\right]_{\mathrm{coll}} = \int\int\int (\delta_1' + \delta_2' - \delta_1 - \delta_2) f_1^{\mathrm{d}} f_2^{\mathrm{MB}} g\sigma\,\mathrm{d}^2\Omega\,\mathrm{d}^3\mathbf{c}_1\,\mathrm{d}^3\,\mathbf{c}_2$$
$$+ \frac{1}{2}\int\int\int (\delta_1' + \delta_2' - \delta_1 - \delta_2) f_1^{\mathrm{d}} f_2^{\mathrm{d}} g\sigma\mathrm{d}^2\Omega\,\mathrm{d}^3\,\mathbf{c}_1\,\mathrm{d}^3\,\mathbf{c}_2 \tag{8}$$

This form of the collision integral suggests that two types of collisions must be considered: those involving a deviational particle and the underlying Maxwell–Boltzmann distribution ($f_1^{\mathrm{MB}} f_2^{\mathrm{d}}$) and representing the linear term $\mathcal{L}^{\mathrm{MB}}(f^{\mathrm{d}})$, and those between two deviational particles ($f_1^{\mathrm{d}} f_2^{\mathrm{d}}$), representing the non-linear term $\mathcal{J}(f^{\mathrm{d}}, f^{\mathrm{d}})$. Let us consider the first type of collision briefly: from (8) we see that particle 1 drawn from f^{d} collides with particle 2 drawn from f^{MB} and leads to the creation of four particles: $\mathrm{sgn}(f_1^{\mathrm{d}})\delta_1'$, $\mathrm{sgn}(f_1^{\mathrm{d}})\delta_2'$, $-\mathrm{sgn}(f_1^{\mathrm{d}})\delta_1$, $-\mathrm{sgn}(f_1^{\mathrm{d}})\delta_2$. The existing particle 2 $[\mathrm{sgn}(f_1^{\mathrm{d}})\delta_2]$ is cancelled by the new $-\mathrm{sgn}(f_1^{\mathrm{d}})\delta_2$ particle, thus leading to a net creation of three particles. The $f_1^{\mathrm{d}} f_2^{\mathrm{d}}$ term can be interpreted and implemented analogously [5,6]. [Note that if $f^{\mathrm{MB}} = 0$, $f^{\mathrm{d}} > 0$, we recover DSMC.]

The deviational scheme just described has already been developed [5,6] and extensively tested. It has been found to be very efficient for $Kn = \lambda_0/L \gtrsim 1$, where L is the flow characteristic lengthscale; in this regime, collisions with the system walls lead to sufficient particle cancellation for the number of deviational particles to stabilize. Unfortunately, for $Kn < 1$ the high rate of intermolecular collisions compared to collisions with the system walls leads to a high net rate of particle creation that results in a divergence in the number of particles, unless a particle cancellation scheme is introduced. Such a scheme was introduced and shown to be capable of stabilizing the calculation [5,6]; unfortunately, particle cancellation schemes effectively introduce a velocity space discretization (with associated numerical error – particularly obvious in the higher moments of the distribution [5,6] – and storage requirements); this is a major disadvantage compared to DSMC, which does not require discretization in velocity space.

The above-described weakness can be overcome by using a new formulation for the collision integral. This formulation, and the resulting *new* particle scheme for solving the Boltzmann equation *which requires no particle cancellation or velocity space discretization*, are discussed in the next section.

4. LVDSMC: low-variance deviational simulation Monte Carlo

LVDSMC is a time explicit particle method for solving the Boltzmann equation which retains the basic algorithmic structure of DSMC. As in DSMC, space is discretized in a number of cells in which the collision process is performed in a space-homogeneous fashion, while time integration is achieved by performing the desired number of timesteps of duration Δt. Each timestep consists of the following substeps:

- Advection substep: Integrate (3) for a time increment Δt. Apply boundary conditions to particles interacting with system boundaries.
- Collision substep: Integrate (4) for a time increment Δt.

In the remainder of this section we will describe the major ingredients of this new method in more detail. We start with the collision substep since this contains the new collision integral formulation which is the core of the new approach. We then discuss the advection substep with particular emphasis on the changes required by the new collision integral formulation.

Extracting hydrodynamic quantities from the simulation can be performed every timestep or whenever required. The process remains largely the same as DSMC with one difference: the contribution of the underlying Maxwell–Boltzmann distribution needs to be added to the sampled results since sampling the deviational particles provides only the contribution of the deviation from equilibrium to hydrodynamic quantities.

4.1. The collision substep

4.1.1. A new collision integral formulation

The proposed technique *rigorously* avoids creating a large fraction of the deviational particles (that would have otherwise been created by the collision process) by "consolidating" their net effect (after all possible cancellation has taken place) into a change in the local Maxwell–Boltzmann distribution.

The new formulation proposed here focuses on a different treatment of the linear part of the collision operator, $\mathcal{L}^{\mathrm{MB}}(f^{\mathrm{d}})$. Focusing on the linear part of the collision operator is not restrictive since the present method has been developed for, and holds an advantage over DSMC, in cases where the deviation from equilibrium is small; this coincides with the regime where the contribution of the second-order term is typically negligible. However, if desired, the proposed method may be extended to include the non-linear part of the collision operator, by treating it as briefly described above and in more detail in previous work [5,6]. Our preliminary results [8] indicate that upon addition of the non-linear term, the number of particles remains bounded for $Ma \lesssim 1$.

We proceed with the treatment of the linear term; unless otherwise stated, our discussion of the collision operator below refers to $\mathcal{L}^{\mathrm{MB}}(f^{\mathrm{d}})$. Particle cancellation at each timestep is achieved by absorbing as large a fraction of the action of the collision operator over one timestep as possible into the underlying local Maxwell–Boltzmann distribution by changing this distribution, and generating deviational particles to represent *only the remaining part* (that cannot be expressed as a change of the local Maxwell–Boltzmann distribution). The rationale for this choice is that the action of the collision operator is to drive the system towards local equilibrium, namely, a Maxwell–Boltzmann distribution. In other words, in a homogeneous calculation starting from a distribution away from equilibrium (and thus some arbitrary distribution of deviational particles) the action of the collision operator should be such that the final state is that of a local Maxwell–Boltzmann distribution – at the (conserved) system mass, momentum and energy–and zero deviational particles. To this end, we write

$$\int_0^{\Delta t} \mathcal{L}^{\mathrm{MB}}(f^{\mathrm{d}})\mathrm{d}t \approx \mathcal{L}^{\mathrm{MB}}(f^{\mathrm{d}})\Delta t = \Delta f^{\mathrm{MB}} + \Delta f^{\mathrm{d}} \tag{9}$$

where

$$\Delta f^{\mathrm{MB}} = \left[\frac{1}{n_{\mathrm{MB}}}\Delta n_{\mathrm{MB}} + 2\frac{\boldsymbol{\omega}}{c_{\mathrm{MB}}^2}\cdot\Delta\mathbf{u}_{\mathrm{MB}} + \frac{1}{c_{\mathrm{MB}}}\left(2\frac{\boldsymbol{\omega}^2}{c_{\mathrm{MB}}^2} - 3\right)\Delta c_{\mathrm{MB}}\right] f^{\mathrm{MB}} \tag{10}$$

and $\boldsymbol{\omega} = \mathbf{c} - \boldsymbol{u}_{\mathrm{MB}}$. In other words, by changing the number density, mean velocity and temperature of the local Maxwell–Boltzmann distribution, we absorb part of the action of the collision integral and, as will be seen later, reduce the number of deviational particles generated drastically. A number of possibilities exist for choosing the amounts Δn_{MB}, $\Delta \mathbf{u}_{\mathrm{MB}}$, Δc_{MB}; the particular choice made in this work is explained below.

We proceed by writing

$$[\mathcal{L}^{\mathrm{MB}}(f^{\mathrm{d}})](\mathbf{c}) = \int K_1(\boldsymbol{\omega}, \boldsymbol{\omega}_1) f^{\mathrm{d}}(\mathbf{c}_1) \mathrm{d}^3\mathbf{c}_1 - \int K_2(\boldsymbol{\omega}, \boldsymbol{\omega}_1) f^{\mathrm{d}}(\mathbf{c}_1) \mathrm{d}^3\mathbf{c}_1 - \nu(\boldsymbol{\omega}) f^{\mathrm{d}}(\mathbf{c}) \tag{11}$$

where

$$K_1(\mathbf{c}, \mathbf{c}_1) = \frac{2 n_{\mathrm{MB}} \mathrm{d}^2}{\sqrt{\pi} c_{\mathrm{MB}}^2} \frac{1}{|\tilde{\mathbf{c}} - \tilde{\mathbf{c}}_1|} \exp\left[-\tilde{\mathbf{c}}^2 + \frac{(\tilde{\mathbf{c}} \times \tilde{\mathbf{c}}_1)^2}{|\tilde{\mathbf{c}} - \tilde{\mathbf{c}}_1|^2} \right] = \frac{2 n_{\mathrm{MB}} \mathrm{d}^2}{\sqrt{\pi} c_{\mathrm{MB}}^2} \frac{1}{|\tilde{\mathbf{c}} - \tilde{\mathbf{c}}_1|} \exp\left[-\frac{[\tilde{\mathbf{c}} \cdot (\tilde{\mathbf{c}} - \tilde{\mathbf{c}}_1)]^2}{|\tilde{\mathbf{c}} - \tilde{\mathbf{c}}_1|^2} \right] \tag{12}$$

$$K_2(\mathbf{c}, \mathbf{c}_1) = \frac{n_{\mathrm{MB}} \mathrm{d}^2}{\sqrt{\pi} c_{\mathrm{MB}}^2} |\tilde{\mathbf{c}} - \tilde{\mathbf{c}}_1| \exp[-\tilde{\mathbf{c}}^2] \tag{13}$$

$$\nu(\mathbf{c}) = \sqrt{\pi} n_{\mathrm{MB}} \mathrm{d}^2 c_{\mathrm{MB}} \left[\exp[-\tilde{\mathbf{c}}^2] + \left(2|\tilde{\mathbf{c}}| + \frac{1}{|\tilde{\mathbf{c}}|} \right) \int_0^{|\tilde{\mathbf{c}}|} \exp[-\xi^2] \mathrm{d}\xi \right] \tag{14}$$

and tilde denotes normalization by c_{MB}, i.e. $\tilde{\mathbf{c}} = \mathbf{c}/c_{\mathrm{MB}}$. These expressions are generalizations [8] of the original expressions [12,2,4] to the case of a Maxwell–Boltzmann distribution for an arbitrary flow velocity. Although as shown in [11] and discussed briefly above, within the linear approximation linearization about a Maxwell–Boltzmann distribution with $\mathbf{u}_{\mathrm{MB}} = 0$ is sufficient, the formulation presented here has the advantage of implementing the linear term exactly, which is theoretically pleasing, but also makes the simulation of non-linear flows possible (provided the effect of $f^{\mathrm{d}} - f^{\mathrm{d}}$ collisions is also added); the disadvantage of the present formulation is that the reference state (c_{MB}, n_{MB}, $\mathbf{u}_{\mathrm{MB}}$) changes during the simulation, thus slightly increasing the algorithmic complexity.

The first term in (11), can be interpreted as the gain term due to both the Maxwell–Boltzmann and the deviational distribution; the second term is the loss term due to the f^{MB} term; the last term is the loss term due to f^{d}. This last term can be directly implemented as a particle sink (deletion). We thus focus on implementing the first two terms in Eq. (11) as a combined particle generation and local Maxwell–Boltzmann distribution change. The amount of change is chosen such that it absorbs the mass, momentum and energy change *due to the action of the first two terms, in the frame of the local Maxwell–Boltzmann distribution*; in other words,

$$\int \Delta f^{\mathrm{MB}} \{1, \boldsymbol{\omega}, |\boldsymbol{\omega}|^2\} \mathrm{d}^3\mathbf{c} = \Delta t \int \int [K_1(\boldsymbol{\omega}, \boldsymbol{\omega}_1) - K_2(\boldsymbol{\omega}, \boldsymbol{\omega}_1)] f^{\mathrm{d}}(\mathbf{c}_1) \{1, \boldsymbol{\omega}, |\boldsymbol{\omega}|^2\} \mathrm{d}^3\mathbf{c}_1 \mathrm{d}^3\mathbf{c} \tag{15}$$

Using the fact that mass, momentum and energy are conserved during collisions, the above leads to the following solution

$$\begin{aligned} \Delta n_{\mathrm{MB}} &= \Delta t \int \nu(\boldsymbol{\omega}_1) f^{\mathrm{d}}(\mathbf{c}_1) \mathrm{d}^3\mathbf{c}_1 \\ \Delta \mathbf{u}_{\mathrm{MB}} &= \frac{\Delta t}{n_{\mathrm{MB}}} \int \boldsymbol{\omega}_1 \nu(\boldsymbol{\omega}_1) f^{\mathrm{d}}(\mathbf{c}_1) \mathrm{d}^3\mathbf{c}_1 \\ \Delta c_{\mathrm{MB}} &= \frac{\Delta t}{3 n_{\mathrm{MB}} c_{\mathrm{MB}}} \int \left[\boldsymbol{\omega}_1^2 - \frac{3}{2} c_{\mathrm{MB}}^2 \right] \nu(\boldsymbol{\omega}_1) f^{\mathrm{d}}(\mathbf{c}_1) \mathrm{d}^3\mathbf{c}_1 \end{aligned} \tag{16}$$

Although other choices for Δf^{MB} are possible, and perhaps superior, the one adopted here is convenient (in terms of allowing the above closed form solution) but also appears to work very well. Moreover, a strong physical justification for this choice exists; it will be more clear after the complete algorithm is described and discussed in Sections 4.1.2 and 4.1.3.

4.1.2. Collision algorithm

Let us define the following short-hand notation:

$$\begin{aligned}\overline{K}_1 f^{\mathrm{d}} &\equiv \int K_1(\boldsymbol{\omega},\boldsymbol{\omega}_1) f^{\mathrm{d}}(\mathbf{c}_1)\mathrm{d}^3\mathbf{c}_1 \\ \overline{K}_2 f^{\mathrm{d}} &\equiv \int K_2(\boldsymbol{\omega},\boldsymbol{\omega}_1) f^{\mathrm{d}}(\mathbf{c}_1)\mathrm{d}^3\mathbf{c}_1 \\ \bar{\nu} f^{\mathrm{d}} &\equiv \nu(\boldsymbol{\omega}) f^{\mathrm{d}}(\mathbf{c})\end{aligned} \tag{17}$$

Using this notation, the linear part of the collision algorithm can then be described as

$$\mathcal{L}^{\mathrm{MB}}(f^{\mathrm{d}})\Delta t = \underbrace{\Delta t[\overline{K}_1 - \overline{K}_2]f^{\mathrm{d}} - \Delta f^{\mathrm{MB}}}_{\text{generation of particles}} + \underbrace{\Delta f^{\mathrm{MB}}}_{\text{changing of the Maxwell–Boltzmann distribution}} - \underbrace{\bar{\nu} f^{\mathrm{d}}\Delta t}_{\text{deletion of particles}}$$

Based on this rearrangement, the collision algorithm proceeds as follows:

- Delete deviational particles of velocity $\mathbf{c}$ with probability proportional to $\nu(\boldsymbol{\omega})\Delta t$.
- Change the underlying Maxwell–Boltzmann distribution by the amount given in Eq. (16). The integrals in (16) are calculated by sampling a subset of the deviational particles in the cell.
- Generate deviational particles according to the distribution

$$\{\Delta t[\overline{K}_1 - \overline{K}_2]f^{\mathrm{d}} - \Delta f^{\mathrm{MB}}\} \tag{18}$$

  This is achieved through an acceptance–rejection technique [8]. The challenge lies in the fact that the explicit functional form of this distribution is not known, but needs to be calculated "on the fly". This is achieved by sampling a subset of the deviational particles in the cell, since evaluating this distribution function will have to be repeated a large number of times. The essence of the acceptance–rejection algorithm is then as follows: we choose randomly N_1 velocities $\mathbf{c}$, which will be the velocities of candidate particles to be created. These velocities are drawn from an arbitrary distribution $g(\mathbf{c})$, which is chosen so as to be greater than $|\Delta t[\overline{K}_1 - \overline{K}_2]f^{\mathrm{d}} - \Delta f^{\mathrm{MB}}|$ for all $\mathbf{c}$; the number of candidate velocities N_1 is equal to $N_{\mathrm{eff}}^{-1}\int g(\mathbf{c})\,\mathrm{d}^3\mathbf{c}$. For a given $\mathbf{c}$, we loop over a number of numerical particles in order to compute $\Delta t[\overline{K}_1 - \overline{K}_2]f_d$ as discussed above. The particle of velocity $\mathbf{c}$ is created if $|\Delta t[\overline{K}_1 - \overline{K}_2]f^{\mathrm{d}} - \Delta f^{\mathrm{MB}}| > \mathcal{R}g(\mathbf{c})$, where $\mathcal{R}$ is a uniform random number in $[0,1]$. The sign of the particle is determined from $\mathrm{sgn}[\Delta t[\overline{K}_1 - \overline{K}_2]f_{\mathrm{d}} - \Delta f^{\mathrm{MB}}]$.

4.1.3. Discussion

It has to be noted that kernel K_1 is singular at the point $\mathbf{c} = \mathbf{c}_1$ and diverges as $1/|\mathbf{c} - \mathbf{c}_1|$. This singularity complicates particle generation through an acceptance/rejection procedure, since this method applies to bounded distributions. To deal with this difficulty, we set a cutoff relative velocity v_{c} and define a modified kernel. The modified kernel is defined such that it is constant $\forall\mathbf{c}$ for which $|\mathbf{c} - \mathbf{c}_1| < v_{\mathrm{c}}$, and equal to the mean value of the kernel over the volume of a sphere centered on $\mathbf{c}_1$, and of radius v_{c}. This mean value is equal [8] to $3n_{\mathrm{MB}}\mathrm{d}^2\mathrm{erf}(\tilde{\mathbf{c}}_1)/(2\mathbf{c}_1 v_{\mathrm{c}})$. Our numerical results are insensitive to the value of v_{c} as long as it is small: in our computations we used $v_{\mathrm{c}} = 0.1c_0$; changing v_{c} to $0.01c_0$ has no discernible effect.

We now discuss, briefly, the rationale for our particular choice for Δf^{MB} given by Eq. (15) and leading to Eq. (16). This choice is based on the following two observations: first, a mechanism for deleting particles exists within the algorithm (namely $\bar{\nu} f^{\mathrm{d}}$); second, in flows where the final distribution is a Maxwell–Boltzmann distribution (say $\check{f}^{\mathrm{MB}}$), if f^{d} is constrained to have no net mass, momentum and energy, it has to be zero since it is also constrained to be equal to the difference of two Maxwell–Boltzmann distributions ($f^{\mathrm{d}} = f - f^{\mathrm{MB}} = \check{f}^{\mathrm{MB}} - f^{\mathrm{MB}}$). In other words, we expect that for problems where a local equilibrium solution exists, through this formulation, the algorithm will be able to arrive at this solution (i.e. $f^{\mathrm{MB}} = \check{f}^{\mathrm{MB}}, f^{\mathrm{d}} = 0$). Given the above, one may expect that in general problems, this method will make f^{MB} go to an appropriate Maxwell–Boltzmann distribution so as to make f^{d} small.

4.2. The advection substep

Recall that in this paper we assume that external fields are zero or negligible. The presence of such fields requires straightforward extensions that will be presented in a future publication.

Using the definition $f^{\mathrm{d}} = f - f^{\mathrm{MB}}$ in (3) yields the following equation:

$$\frac{\partial f^{\mathrm{d}}}{\partial t} + \mathbf{c}\cdot\frac{\partial f^{\mathrm{d}}}{\partial \mathbf{r}} = -\mathbf{c}\cdot\frac{\partial f^{\mathrm{MB}}}{\partial \mathbf{r}} \tag{19}$$

governing the deviational distribution function during the advection substep. This equation shows that if f^{MB} is independent of space, the advection substep for deviational particles is identical to that of physical (DSMC) particles. Here, however, we allow f^{MB} to vary between cells, leading to discontinuities of this function at the boundaries between cells which leads to fluxes of deviational particles across these boundaries.

The solution to this equation can be written as a superposition of a free molecular advection for the deviational particles (solution of the homogeneous equation) and a correction term accounting for the contribution of the right-hand-side. The latter is implemented as a deviational particle flux term at cell boundaries, as explained in detail below.

In summary, the advection substep consists of the following steps:

- Free molecular advection of deviational particles.
- Generation and advection of deviational particles at cell interfaces to ensure molecular flux conservation as required by the inhomogeneous term in (19).
- Imposition of boundary conditions for particles interacting with system boundaries.

Below we discuss the last two steps in more detail.

4.2.1. Ensuring molecular flux conservation

To simplify the notation and *without loss of generality* let us assume that the interface between two cells contains the origin $\mathbf{r} = 0$. The term $-\mathbf{c}\cdot\partial f^{\mathrm{MB}}/\partial\mathbf{r}$ can be evaluated to $(\mathbf{c}\cdot\mathbf{n})(f^{\mathrm{MB}(l)} - f^{\mathrm{MB}(r)})\delta(\mathbf{n}\cdot\mathbf{r})$, where $\mathbf{n}$ denotes the unit normal to the interface, and l and r denote the "left" ($\mathbf{n}\cdot\mathbf{r} < 0$) and "right" ($\mathbf{n}\cdot\mathbf{r} > 0$) cell, respectively. The particular solution of (19) due to this term is

$$\begin{cases} [f^{\mathrm{MB}(l)}(\mathbf{c}) - f^{\mathrm{MB}(r)}(\mathbf{c})]\mathrm{sgn}(\mathbf{c}\cdot\mathbf{n}) & \text{if } 0 \leqslant (\mathbf{n}\cdot\mathbf{r})/(\mathbf{c}\cdot\mathbf{n}) \leqslant \Delta t \\ 0 & \text{otherwise} \end{cases}$$

The distribution of deviational particles corresponding to this solution can be generated using a variety of methods including a modification of the "reservoir" approach widely used in DSMC to model open boundaries [24]. In the present work, we generate the required deviational particles by drawing particles from the (fluxal) distribution

$$(\mathbf{c}\cdot\mathbf{n})[f^{\mathrm{MB}(l)}(\mathbf{c}) - f^{\mathrm{MB}(r)}(\mathbf{c})] \tag{20}$$

and spreading them out over a domain $0 \leqslant (\mathbf{n}\cdot\mathbf{r})/(\mathbf{c}\cdot\mathbf{n}) \leqslant \Delta t$ by advecting them for a randomly chosen fraction of a timestep.

In order to treat the most general case, in the present work, generating particles according to (20) is accomplished using the acceptance–rejection scheme described below and in [8]. Note, however, that in a number of cases of practical interest e.g. isothermal flow with no flow normal to cell interface, generation of the velocity components directly from the desired distribution is possible, leading to a significantly more efficient implementation. Generation of the fluxes due to $f^{\mathrm{MB}(l)}$ and $f^{\mathrm{MB}(r)}$ separately using standard (and efficient) DSMC methods and allowing the resulting particles to cancel as a result of the action of the collision operator is another possibility that merits investigation.

Let $\mathcal{R}_1$ and $\mathcal{R}_2$ denote random numbers uniformly distributed in $[0, 1]$, S be the area of the cell interface and $V_{\mathbf{c}} = 8c_{\max}^3$. Also, let M be the ceiling of the function $|(\mathbf{c}\cdot\mathbf{n})[f^{\mathrm{MB}(l)}(\mathbf{c}) - f^{\mathrm{MB}(r)}(\mathbf{c})]|$ and $c_{\max}$ a cutoff velocity such that the value of the distribution (20) is negligible if the absolute value of any of the components of $\mathbf{c}$ exceeds $c_{\max}$. The acceptance–rejection technique used here can be summarized as follows:

- Repeat $N = \mathrm{SMV}_{\mathbf{c}}\Delta t/N_{\mathrm{eff}}$ times

– Choose a candidate velocity $\mathbf{c}_c$ where each component is chosen from a uniform distribution in $[-c_{max}, c_{max}]$
– If $|(\mathbf{c}\cdot\mathbf{n})[f^{MB(l)}(\mathbf{c}) - f^{MB(r)}(\mathbf{c})]| > \mathcal{R}_1 M$, create a particle
  * of velocity $\mathbf{c}_c$
  * of sign $\mathrm{sgn}[(\mathbf{c}_c\cdot\mathbf{n})[f^{MB(l)}(\mathbf{c}_c) - f^{MB(r)}(\mathbf{c}_c)]$
  * at a position such that $\mathbf{n}\cdot\mathbf{r} = \Delta t(\mathbf{c}_c\cdot\mathbf{n})\mathcal{R}_2$

4.2.2. Boundary conditions

In this work we consider diffuse boundary conditions, although the method is in no way limited to these; extensions to other wall boundary conditions will be presented in a future publication. The boundary treatment requires consideration of both deviational particles and the flux of particles due to the underlying f^{MB}.

More specifically, the wall distribution, parametrized by the wall properties $\boldsymbol{u}_{wall}, c_{wall} = \sqrt{2kT_{wall}/m}$ and n_{wall}, is written as $f^{wall} = n_{wall}F^{wall}(\mathbf{c}) = n_{wall}(\pi c_{wall}^2)^{-3/2}\exp[-(\mathbf{c}-\boldsymbol{u}_{wall})^2/c_{wall}^2]$, where the quantity n_{wall} is determined by the requirement that the mass flux into the wall is equal to the mass flux leaving the wall. The algorithm used here for evaluating n_{wall} considers deviational particles and the flux of particles due to the underlying f^{MB} separately – by writing $n_{wall} = n_{wall}^{MB} + n_{wall}^{d}$ and evaluating each term from the corresponding mass-flux balance – and is an adaptation of the algorithm already explained in detail before [5,6,8].

In the case of deviational particles colliding with the wall, the algorithm is much like that of DSMC, except pairs consisting of a positive and negative particle can be cancelled because it is only the *net* mass flux (determining n_{wall}^{d}) that is of interest. The net number of deviational particles striking the wall is sent back into the domain drawn from $F^{wall}(\mathbf{c})$.

The effect of the underlying Maxwell–Boltzmann distribution is more subtle; the presence of this distribution implies both a molecular flux incident upon the wall, and a molecular flux leaving the wall. Thus, deviational particles need to be *created* according to the distribution given by the difference between the wall distribution $[n_{wall}^{MB}F^{wall}(\mathbf{c})]$ and the underlying Maxwell–Boltzmann distribution of the neighboring cell $[f^{MB(r)}(\mathbf{c})]$, as described in Section 4.2.1; here, we have again assumed, without loss of generality, that the interface between the wall and the neighboring cell contains the origin $\mathbf{r} = 0$ and that the wall extends over $\mathbf{n}\cdot\mathbf{r} \leqslant 0$. Following the result of Section 4.2.1, deviational particles entering the domain from the wall ($\mathbf{c}\cdot\mathbf{n} > 0$) are drawn from $(\mathbf{c}\cdot\mathbf{n})[n_{wall}^{MB}F^{wall}(\mathbf{c}) - f^{MB(r)}(\mathbf{c})]$ and are spread out into the region $0 \leqslant \mathbf{n}\cdot\mathbf{r} \leqslant (\mathbf{c}\cdot\mathbf{n})\Delta t$ by being advected for a random fraction of a timestep. Here, n_{wall}^{MB} is determined from

$$\int_{\mathbf{c}\cdot\mathbf{n}<0}(\mathbf{c}\cdot\mathbf{n})f^{MB(r)}(\mathbf{c})\mathrm{d}^3\mathbf{c} = \int_{\mathbf{c}\cdot\mathbf{n}>0}(\mathbf{c}\cdot\mathbf{n})n_{wall}^{MB}F^{wall}(\mathbf{c})\mathrm{d}^3\mathbf{c} \tag{21}$$

5. Numerical results

5.1. Validation

We performed a number of tests to validate this method; all tests yielded excellent agreement with DSMC solutions. Below we present a representative sample of our validation results. In all our calculations, integrals (16) and (17) were evaluated by randomly sampling 100 particles in each cell, and all particles when the number of particles was smaller than 100.

To isolate the effects of collisions and thus validate the new treatment of the collision integral, we study the homogeneous relaxation of the gas from an initial condition of

$$f^i = \frac{n_0}{2(\pi c_0^2)^{3/2}}\left[\exp\left(-\frac{(c_x-\alpha)^2 + c_y^2 + c_z^2}{c_0^2}\right) + \exp\left(-\frac{(c_x+\alpha)^2 + c_y^2 + c_z^2}{c_0^2}\right)\right] \tag{22}$$

The initial number of particles was approximately 9250. We monitor the relaxation by plotting the evolution of $\langle c_x^4\rangle$ as a function of time (due to mass, momentum, and energy conservation as well as symmetry consid-

erations, lower moments provide less interesting variations). This test highlights the basic principle on which LVDSMC is based: starting from an initial $f^{\mathrm{MB}} = f^0$ and a number of deviational particles representing $f^i - f^0$, the simulation proceeds to a final equilibrium state characterized by a Maxwell–Boltzmann distribution at the final temperature, given by $T_f = T_0 + m\alpha^2/(3k)$, and zero deviational particles. A comparison between LVDSMC and DSMC results for $m\alpha^2/(3kT_0) = 0.0048$ is shown in Fig. 1. The agreement is excellent.

We also performed a number of validation tests for spatially dependent problems. Here we show LVDSMC results for an impulsively started shear flow, in which at time $t = 0$ two infinite, diffuse walls in the y–z plane and at $x = 0$ and $x = L$ respectively, start moving in the y-direction with velocities $\pm U$. Figs. 2–4 show a comparison with DSMC results at different Knudsen numbers (Kn) for the normalized flow velocity u_y/U and shear stress $\tau_{xy}/(\rho c_0^2)$ at various time instants, including steady state for $Kn = 1$ and $Kn = 10$. The same spatial and time discretization as well as comparable number of simulation particles was used in the two methods. The agreement between the results is excellent.

Fig. 5 shows the evolution of the number of particles in two cells in a $Kn = 1$ calculation. The figure shows that under the new collision integral formulation, the number of particles per cell becomes constant at steady state.

5.2. Quantifying the variance reduction

In this section we report on the variance reduction (compared to DSMC) observed in our LVDSMC simulations. When the deviation from equilibrium is small, the statistical uncertainty in DSMC is dominated by the equilibrium fluctuations and does not depend on the deviation from equilibrium. On the contrary, in LVDSMC the statistical uncertainty depends on the local deviation from equilibrium. Thus, to facilitate comparison, we have chosen to report the variance reduction observed in steady shear flows. Characterization of the variance reduction in more complex flows as well as theoretical analysis of the statistical uncertainty in LVDSMC will be undertaken in future work.

We have performed comparisons for both the flow velocity and the shear stress. Fig. 6 presents simulation results for the variance reduction in the flow velocity achieved by LVDSMC at two different Knudsen numbers, namely $Kn = 0.4$ and $Kn = 2.5$. The figure reports $R_u = \mathrm{Var}^{\mathrm{DSMC}}(u_y)/\mathrm{Var}^{\mathrm{LVDSMC}}(u_y)$, where $\mathrm{Var}(u_y)$ is

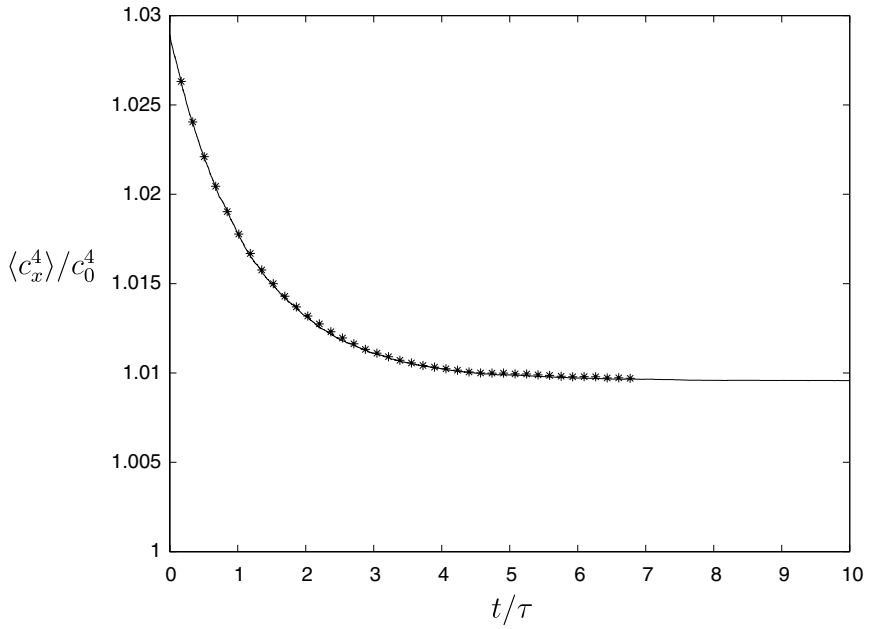

Fig. 1. Comparison between DSMC (stars) and LVDSMC (solid line) results for homogeneous relaxation from initial distribution f^i.

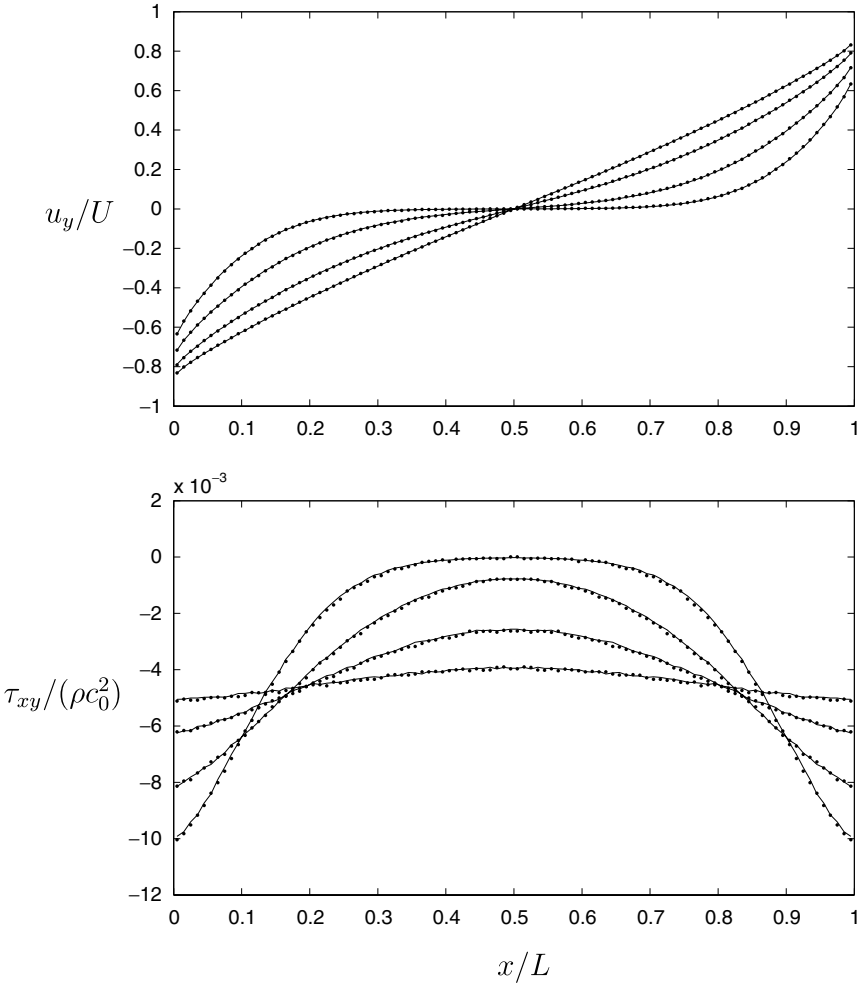

Fig. 2. Velocity profiles (top) and shear stress profiles (bottom) in impulsively started shear flow ($Kn = 0.1$, $U = 0.05c_0$) at various times. The continuous line represents the present method, while dots represent standard DSMC results.

the variance in the cell-averaged flow velocity observed in an ensemble of calculations. Fig. 7 presents simulation results for the variance reduction in the shear stress achieved by LVDSMC, for the same Knudsen numbers; it reports $R_\tau = \mathrm{Var}^{\mathrm{DSMC}}(\tau_{xy})/\mathrm{Var}^{\mathrm{LVDSMC}}(\tau_{xy})$, where $\mathrm{Var}(\tau_{xy})$ is the variance in the cell-averaged shear stress observed in an ensemble of calculations. $\mathrm{Var}^{\mathrm{DSMC}}(u_y)$ and $\mathrm{Var}^{\mathrm{DSMC}}(\tau_{xy})$ have been calculated using equilibrium statistical mechanics [10]; the theory used neglects the contribution of the deviation from equilibrium (this is an excellent approximation in DSMC as our results confirm).

R is a measure of the theoretical reduction in computational cost achieved by LVDSMC. The figures show that, as expected, the variance reduction (and thus the computational savings) grow as Ma^{-2} for $Ma \to 0$. They also show that the variance reduction is weakly dependent on the Knudsen number and that the variance reduction in the flow velocity is slightly higher than the variance reduction in the shear stress.

The actual cost of our LVDSMC simulations is artificially inflated due to the use of very inefficient acceptance–rejection techniques (with very conservative upper bounds) both in the collision and advection routines. Despite this, in our validation simulations of Section 5.1 where DSMC and LVDSMC simulations were run with the same discretization, we observed a speedup of at least one order of magnitude (these tests were performed at $U = \pm 0.05c_0$, the lowest value of U that we could simulate to the desired statistical uncertainty using DSMC). We expect the speedup to be much closer to the theoretical values once tight bounds for the accep-

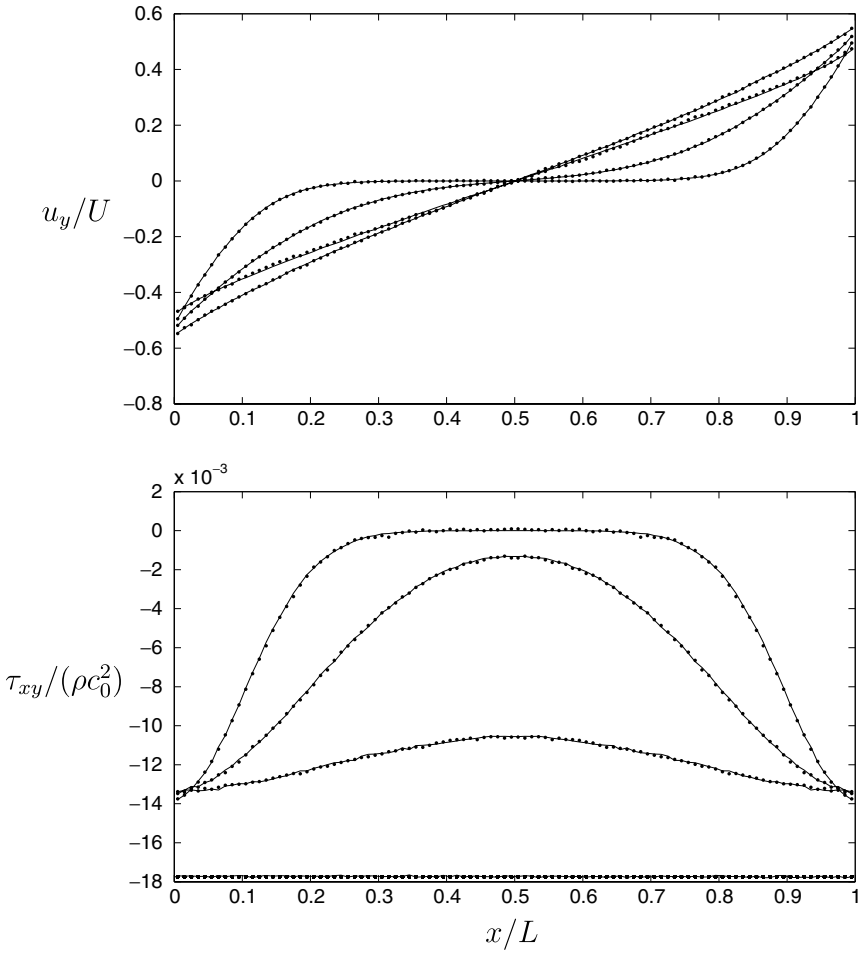

Fig. 3. Velocity profiles (top) and shear stress profiles (bottom) in impulsively started shear flow ($Kn = 1$, $U = 0.05c_0$) at various times. The continuous line represents the present method, while dots represent standard DSMC results.

tance rejection approaches (e.g. by making $M = M(\mathbf{c})$ and modifying the procedure accordingly in Section 4.2) or direct methods for generating random numbers from the desired distribution are implemented.

Finally, we remark that, assuming that for $U > 0.05c_0$ the non-linear effects do not drastically alter the trend shown by Figs. 6 and 7, these results suggest that LVDSMC may hold a computational advantage over DSMC well into the weakly non-linear regime.

6. Final remarks

As briefly discussed in Section 4.1, the linear form of the collision integral given in (11) differs from previous expositions [2,4] where it is simplified by assuming that the Maxwell–Boltzmann distribution has zero macroscopic velocity ($\mathbf{u}_{\mathrm{MB}} = 0$). As stated above, we have retained a more general formulation for a number of reasons: because our underlying Maxwell–Boltzmann distribution evolves during the simulation, the linear formulation about the current f^{MB} has the advantage of being physically consistent. Moreover, it does not neglect any second-order term and it can be combined with an implementation of the quadratic term $[\mathcal{J}(f^{\mathrm{d}}, f^{\mathrm{d}})]$ to provide solutions of the full Boltzmann equation (e.g. for weakly non-linear flows). If none

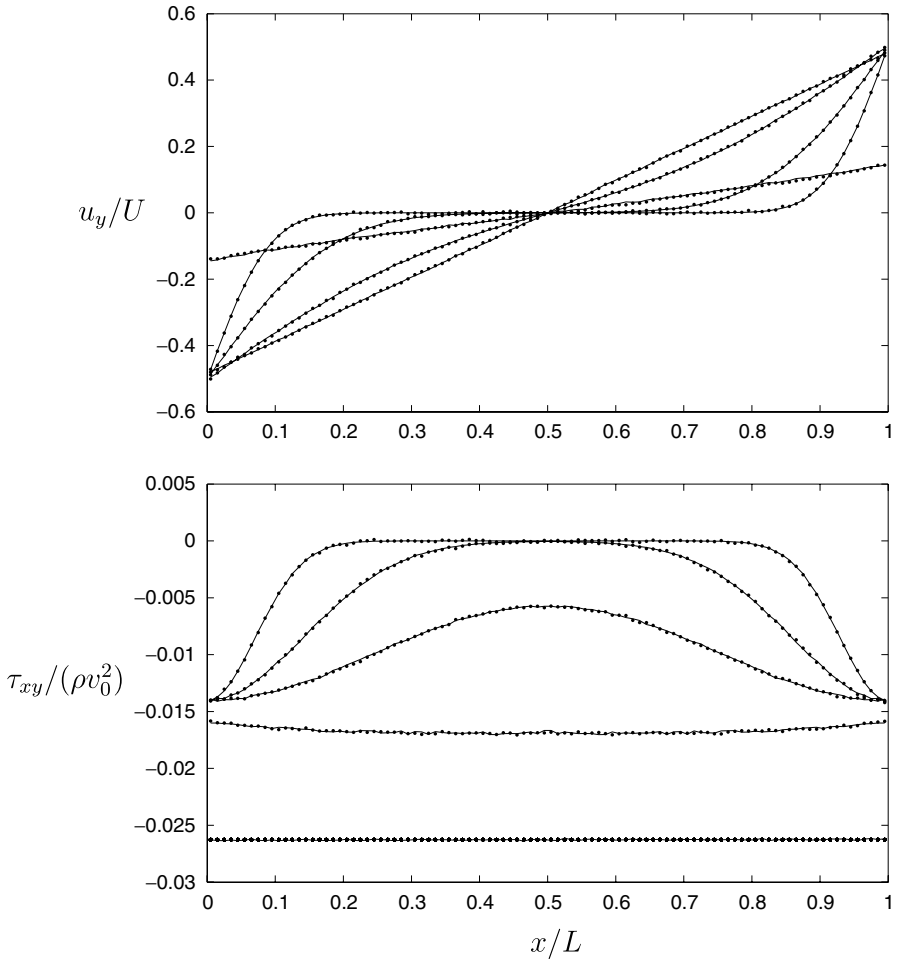

Fig. 4. Velocity profiles (top) and shear stress profiles (bottom) in impulsively started shear flow ($Kn = 10$, $U = 0.05c_0$) at various times. The continuous line represents the present method, while dots represent standard DSMC results.

of these features are of interest, and the local Maxwell–Boltzmann distribution is expected to remain close to the original one, the algorithm may be simplified by linearizing the collision integral about global equilibrium, $f^0(\mathbf{c}) = n_0(\pi c_0^2)^{-3/2}\exp[-\hat{\mathbf{c}}^2]$, to obtain

$$\mathcal{L}^0(f^{\mathrm{d}}) = \int K_1^0(\mathbf{c},\mathbf{c}_1)f^{\mathrm{d}}(\mathbf{c}_1)\mathrm{d}^3\mathbf{c}_1 - \int K_2^0(\mathbf{c},\mathbf{c}_1)f^{\mathrm{d}}(\mathbf{c}_1)\mathrm{d}^3\mathbf{c}_1 - \nu^0(\mathbf{c})f^{\mathrm{d}}(\mathbf{c}) \tag{23}$$

where $\hat{\mathbf{c}} = \mathbf{c}/c_0$, and K_1^0, K_2^0 and ν^0 can be obtained by substituting $n_{\mathrm{MB}} \to n_0$, $c_{\mathrm{MB}} \to c_0$ and $\tilde{\mathbf{c}} \to \hat{\mathbf{c}}$ in the expressions for K_1, K_2 and ν, respectively. Complete expressions for K_1^0, K_2^0 and ν^0 can also be found in the Appendix.

Note that linearization about global equilibrium is possible because

$$\mathcal{L}^0(f^{\mathrm{d}}) = \mathcal{L}^0(f - f^{\mathrm{MB}}) = \mathcal{L}^0(f - f^0) - \mathcal{L}^0(f^{\mathrm{MB}} - f^0) \tag{24}$$

and the last term is of second order since $\mathcal{L}^0(f^{\mathrm{MB}} - f^0) + \mathcal{J}(f^{\mathrm{MB}} - f^0, f^{\mathrm{MB}} - f^0) = 0$. In a similar fashion, under these conditions, the algorithm may be further simplified by taking $\boldsymbol{\omega} \to \mathbf{c}$ in Eqs. (15) and (16) (and Eq. (17)).

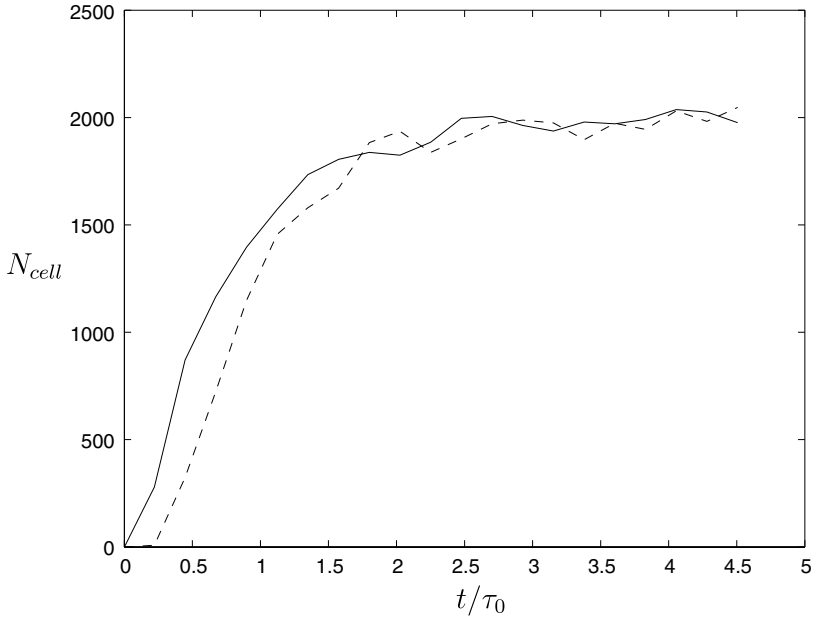

Fig. 5. Number of particles in a cell as a function of time for a $Kn = 1$ calculation. Solid line denotes cell centered on $x = -0.31$ and dashed line denotes cell centered on $x = -0.11$.

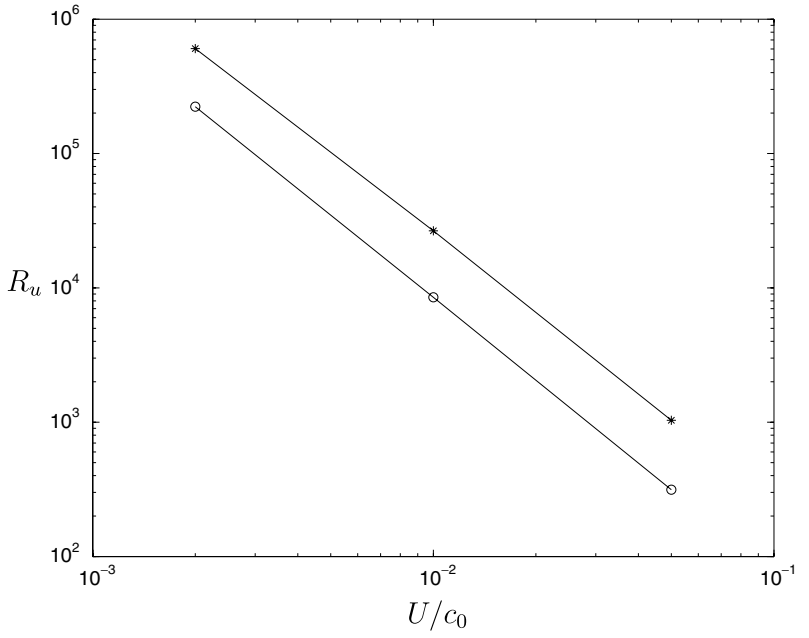

Fig. 6. Variance reduction in steady Couette flow at $Kn = 0.4$ (stars) and $Kn = 2.5$ (circles). R_u is the ratio of the variance in flow velocity in DSMC and LVDSMC calculations (using the same number of particles per cell). Numerical data for the LVDSMC results were obtained with approximately 650 particles per cell.

This approach has been presented and validated in [11] using the same problems as the ones presented above. Similarly excellent agreement with DSMC results is observed.

The addition of the non-linear collision term will be presented in a future publication.

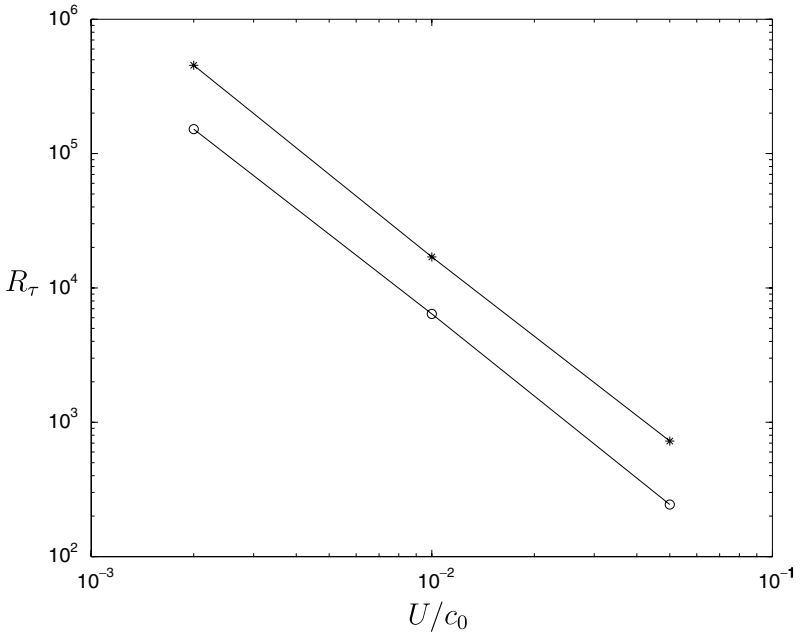

Fig. 7. Variance reduction in steady Couette flow at $Kn = 0.4$ (stars) and $Kn = 2.5$ (circles). R_τ is the ratio of the variance in shear stress in DSMC and LVDSMC calculations (using the same number of particles per cell). Numerical data for the LVDSMC results were obtained with approximately 650 particles per cell.

7. Conclusions

In summary, we have developed a new particle method for solving the Boltzmann equation. This method can capture arbitrarily small deviations from equilibrium at constant computational cost; this is achieved by simulating only the deviation from equilibrium. The method is closely related to DSMC and deviates only in ways necessary to consider the deviation from equilibrium. A very important feature of this method is that, similarly to DSMC, it requires no discretization in the particle velocities (e.g. for particle cancellation). In LVDSMC this is achieved by writing the action of the collision integral in the form of a change in the local equilibrium distribution function (representing the net effect of cancellation of a number of deviational particles) and an "irreducible" set of deviational particles (the remaining particles that cannot be cancelled).

LVDSMC has been validated using DSMC solutions of homogeneous relaxation model-problems and space-dependent time-evolving flows. The validation results show that, compared to DSMC, LVDSMC can achieve comparable accuracy using comparable discretization at significantly smaller computational cost in the limit of low-speed flows, due to the significantly lower statistical uncertainty resulting from simulating only the deviation from equilibrium.

Extension of LVDSMC to interaction models beyond the hard-sphere model as well as theoretical characterization of the statistical uncertainty associated with this method will be the subject of future work.

Acknowledgments

This work was supported, in part, by Sandia National Laboratory. The authors are grateful to L.L. Baker for invaluable help with the formulation of the problem and the calculations. The authors would also like to thank the Associate Editor, Professor P. Degond, for bringing the work on gyrokinetic equations to their attention.

Appendix A. Kernels for a shifted Maxwell–Boltzmann distribution ($u_{\mathrm{MB}} \neq 0$)

We start with the linearized form of the collision integral about a Maxwell–Boltzmann distribution f^{MB}

$$\mathcal{L}^{\mathrm{MB}}(f^{\mathrm{d}}) = \int\int\int (\delta_2' + \delta_1' - \delta_2 - \delta_1) f_1^{\mathrm{d}} f_2^{\mathrm{MB}} g\sigma \,\mathrm{d}^2\Omega \mathrm{d}^3\mathbf{c}_1 \,\mathrm{d}^3\,\mathbf{c}_2 \tag{25}$$

It is known [12,2,4] that when the equilibrium state is that of global equilibrium, $f^0(\mathbf{c}) = (\pi c_0^2)^{-3/2}\exp(-\hat{\mathbf{c}}^2)$, the collision integral can be written as

$$\mathcal{L}^0(f^{\mathrm{d}}) = \int K_1^0(\mathbf{c},\mathbf{c}_1) f^{\mathrm{d}}(\mathbf{c}_1)\mathrm{d}^3\mathbf{c}_1 - \int K_2^0(\mathbf{c},\mathbf{c}_1) f^{\mathrm{d}}(\mathbf{c}_1)\mathrm{d}^3\mathbf{c}_1 - \nu^0(\mathbf{c}) f^{\mathrm{d}}(\mathbf{c}) \tag{26}$$

where the kernels K_1^0, K_2^0 and the collision frequency ν^0 are given below.

Here we give the form of this expression when the local Maxwell–Boltzmann distribution is given by the more general expression $f^{\mathrm{MB}} = n_{\mathrm{MB}}(\pi c_{\mathrm{MB}}^2)^{-3/2}\exp[-(\mathbf{c}-\boldsymbol{u}_{\mathrm{MB}})^2/c_{\mathrm{MB}}^2] = n_{\mathrm{MB}}(\pi c_{\mathrm{MB}}^2)^{-3/2}\exp[-\tilde{\boldsymbol{\omega}}^2]$.

We will be using the fact that, for a given set of precollision and postcollision velocities, $\mathbf{c}_1, \mathbf{c}_2 \to \mathbf{c}_1', \mathbf{c}_2'$, in a frame moving with velocity $\mathbf{u}_{\mathrm{MB}}$ we can write $\boldsymbol{\omega}_1, \boldsymbol{\omega}_2 \to \boldsymbol{\omega}_1', \boldsymbol{\omega}_2'$, where $\boldsymbol{\omega}_i = \mathbf{c}_i - \mathbf{u}_{\mathrm{MB}}$, $\boldsymbol{\omega}_i' = \mathbf{c}_i' - \mathbf{u}_{\mathrm{MB}}$ and $i = 1, 2$.

A.1. Kernel K_2

Kernel K_2 comes from the term

$$-\int\int\int \delta_2 f_1^{\mathrm{d}} f_2^{\mathrm{MB}} g\sigma \,\mathrm{d}^2\Omega \,\mathrm{d}^3\,\mathbf{c}_1 \,\mathrm{d}^3\,\mathbf{c}_2 = -\int\int f^{\mathrm{d}}(\mathbf{c}_1) f^{\mathrm{MB}}(\mathbf{c}) |\mathbf{c}-\mathbf{c}_1| \sigma \,\mathrm{d}^2\Omega \,\mathrm{d}^3\,\mathbf{c}_1 \tag{27}$$

When $f^{\mathrm{MB}}(\mathbf{c}) = f^0(\mathbf{c}) = n_0(\pi c_0^2)^{-3/2}\exp[-\hat{\mathbf{c}}^2]$, Eq. (27) becomes

$$-\int\int f^{\mathrm{d}}(\mathbf{c}_1) n_0 (\pi c_0^2)^{-3/2}\exp[-\hat{\mathbf{c}}^2]|\mathbf{c}-\mathbf{c}_1|\sigma \,\mathrm{d}^2\Omega \,\mathrm{d}^3\,\mathbf{c}_1$$

and kernel K_2^0 can be identified as

$$K_2^0(\mathbf{c},\mathbf{c}_1) = \frac{n_0 \mathrm{d}^2}{\sqrt{\pi c_0^2}} |\hat{\mathbf{c}} - \hat{\mathbf{c}}_1| \exp[-\hat{\mathbf{c}}^2]$$

When $f^{\mathrm{MB}}(\mathbf{c}) = n_{\mathrm{MB}}(\pi c_{\mathrm{MB}}^2)^{-3/2}\exp[-\tilde{\boldsymbol{\omega}}^2]$, Eq. (27) becomes

$$\begin{aligned} &-\int\int f^{\mathrm{d}}(\mathbf{c}_1) n_{\mathrm{MB}}(\pi c_{\mathrm{MB}}^2)^{-3/2}\exp[-\tilde{\boldsymbol{\omega}}^2]|\mathbf{c}-\mathbf{c}_1|\sigma \,\mathrm{d}^2\Omega \,\mathrm{d}^3\,\mathbf{c}_1 \\ &\quad = -\int\int f^{\mathrm{d}}(\mathbf{c}_1) n_{\mathrm{MB}}(\pi c_{\mathrm{MB}}^2)^{-3/2}\exp[-\tilde{\boldsymbol{\omega}}^2]|\boldsymbol{\omega}-\boldsymbol{\omega}_1|\sigma \,\mathrm{d}^2\Omega \,\mathrm{d}^3\,\mathbf{c}_1 = -\int K_2(\boldsymbol{\omega},\boldsymbol{\omega}_1) f^{\mathrm{d}}(\mathbf{c}_1)\mathrm{d}^3\mathbf{c}_1 \end{aligned}$$

A.2. Kernel K_1

Kernel K_1 results from the "gain" term

$$\int\int\int (\delta_2' + \delta_1') f_1^{\mathrm{d}} f_2^{\mathrm{MB}} g\sigma \,\mathrm{d}^2\Omega \,\mathrm{d}^3\,\mathbf{c}_1 \,\mathrm{d}^3\,\mathbf{c}_2 \tag{28}$$

When $f^{\mathrm{MB}}(\mathbf{c}) = f^0(\mathbf{c}) = n_0(\pi c_0^2)^{-3/2}\exp[-\hat{\mathbf{c}}^2]$, Eq. (28) becomes

$$\int\int\int [\delta(\mathbf{c}_1' - \mathbf{c}) + \delta(\mathbf{c}_2' - \mathbf{c})] n_0 (\pi c_0^2)^{-3/2}\exp[-\hat{\mathbf{c}}_2^2] f^{\mathrm{d}}(\mathbf{c}_1)|\mathbf{c}_1 - \mathbf{c}_2|\sigma \,\mathrm{d}^2\Omega \,\mathrm{d}^3\,\mathbf{c}_1 \,\mathrm{d}^3\,\mathbf{c}_2$$

which can be shown [8,2] to equal

$$\int K_1^0(\mathbf{c},\mathbf{c}_1) f^{\mathrm{d}}(\mathbf{c}_1)\,\mathrm{d}^3\,\mathbf{c}_1$$

with

$$K_1^0(\mathbf{c},\mathbf{c}_1)=\frac{2n_0\mathrm{d}^2}{\sqrt{\pi}c_0^2}\frac{1}{|\hat{\mathbf{c}}-\hat{\mathbf{c}}_1|}\exp\left[-\hat{\mathbf{c}}^2+\frac{(\hat{\mathbf{c}}\times\hat{\mathbf{c}}_1)^2}{|\hat{\mathbf{c}}-\hat{\mathbf{c}}_1|^2}\right]$$

When $f^{\mathrm{MB}}(\mathbf{c})=n_{\mathrm{MB}}(\pi c_{\mathrm{MB}}^2)^{-3/2}\exp[-\tilde{\boldsymbol{\omega}}^2]$, Eq. (28) becomes

$$\begin{aligned}&\int\int\int[\delta(\mathbf{c}_1'-\mathbf{c})+\delta(\mathbf{c}_2'-\mathbf{c})]n_{\mathrm{MB}}(\pi c_{\mathrm{MB}}^2)^{-3/2}\exp[-\tilde{\boldsymbol{\omega}}_2^2]f^{\mathrm{d}}(\mathbf{c}_1)|\mathbf{c}_1-\mathbf{c}_2|\sigma\,\mathrm{d}^2\Omega\,\mathrm{d}^3\,\mathbf{c}_1\,\mathrm{d}^3\mathbf{c}_2\\&=\int\int\int[\delta(\boldsymbol{\omega}_1'-\boldsymbol{\omega})+\delta(\boldsymbol{\omega}_2'-\boldsymbol{\omega})]n_{\mathrm{MB}}(\pi c_{\mathrm{MB}}^2)^{-3/2}\exp[-\tilde{\boldsymbol{\omega}}_2^2]f^{\mathrm{d}}(\mathbf{c}_1)|\boldsymbol{\omega}_1-\boldsymbol{\omega}_2|\sigma\,\mathrm{d}^2\Omega\,\mathrm{d}^3\,\boldsymbol{\omega}_1\mathrm{d}^3\boldsymbol{\omega}_2\\&=\int K_1(\boldsymbol{\omega},\boldsymbol{\omega}_1)f^{\mathrm{d}}(\mathbf{c}_1)\mathrm{d}^3\boldsymbol{\omega}_1=\int K_1(\boldsymbol{\omega},\boldsymbol{\omega}_1)f^{\mathrm{d}}(\mathbf{c}_1)\mathrm{d}^3\mathbf{c}_1\end{aligned}$$

A.3. Collision frequency function (ν)

The function ν is derived from the term

$$-\int\int\int\delta_1 f_1^{\mathrm{d}}f_2^{\mathrm{MB}}g\sigma\,\mathrm{d}^2\Omega\mathrm{d}^3\mathbf{c}_1\,\mathrm{d}^3\,\mathbf{c}_2=-f^{\mathrm{d}}(\mathbf{c})\int\int f^{\mathrm{MB}}(\mathbf{c}_2)|\mathbf{c}-\mathbf{c}_2|\sigma\,\mathrm{d}^2\Omega\,\mathrm{d}^3\,\mathbf{c}_2 \tag{29}$$

When $f^{\mathrm{MB}}(\mathbf{c})=f^0(\mathbf{c})=n_0(\pi c_0^2)^{-3/2}\exp[-\hat{\mathbf{c}}^2]$, Eq. (29) becomes

$$-f^{\mathrm{d}}(\mathbf{c})\int\int n_0(\pi c_0^2)^{-3/2}\exp[-\hat{\mathbf{c}}_2^2]|\mathbf{c}-\mathbf{c}_2|\sigma\,\mathrm{d}^2\Omega\,\mathrm{d}^3\,\mathbf{c}_2=-\nu^0(\mathbf{c})f^{\mathrm{d}}(\mathbf{c})$$

and the collision frequency $\nu^0(\mathbf{c})$ can be identified as

$$\nu^0(\mathbf{c})=\int\int n_0(\pi c_0^2)^{-3/2}\exp[-\hat{\mathbf{c}}_2^2]|\mathbf{c}-\mathbf{c}_2|\sigma,\mathrm{d}^2\Omega\,\mathrm{d}^3\,\mathbf{c}_2=\sqrt{\pi}n_0\,\mathrm{d}^2c_0\left[\exp[-\hat{\mathbf{c}}^2]+\left(2\hat{\mathbf{c}}+\frac{1}{\hat{\mathbf{c}}}\right)\int_0^{|\hat{\mathbf{c}}|}\exp[-\xi^2]\mathrm{d}\xi\right]$$

When $f^{\mathrm{MB}}(\mathbf{c})=n^{\mathrm{MB}}(\pi c_{\mathrm{MB}}^2)^{-3/2}\exp[-\tilde{\boldsymbol{\omega}}^2]$, Eq. (29) becomes

$$\begin{aligned}&-f^{\mathrm{d}}(\mathbf{c})\int\int n_{\mathrm{MB}}(\pi c_{\mathrm{MB}}^2)^{-3/2}\exp[-\tilde{\boldsymbol{\omega}}_2^2]|\mathbf{c}-\mathbf{c}_2|\sigma\,\mathrm{d}^2\Omega\,\mathrm{d}^3\,\mathbf{c}_2\\&=-f^{\mathrm{d}}(\mathbf{c})\int\int n_{\mathrm{MB}}(\pi c_{\mathrm{MB}}^2)^{-3/2}\exp[-\tilde{\boldsymbol{\omega}}_2^2]|\boldsymbol{\omega}-\boldsymbol{\omega}_2|\sigma\,\mathrm{d}^2\Omega\,\mathrm{d}^3\,\boldsymbol{\omega}_2=-\nu(\boldsymbol{\omega})f^{\mathrm{d}}(\mathbf{c})\end{aligned}$$

References

[1] W.G. Vincenti, C.H. Kruger, Introduction to Physical Gas Dynamics, Krieger, Florida, 1965.
[2] C. Cercignani, The Boltzmann Equation and its Applications, Springer-Verlag, New York, 1988.
[3] L.L. Baker, N.G. Hadjiconstantinou, Variance reduction for Monte Carlo solutions of the Boltzmann Equation, Phys. Fluids 17 (2005) 051703.
[4] Y. Sone, Kinetic Theory and Fluid Dynamics, Birkhauser, 2002.
[5] L.L. Baker, N.G. Hadjiconstantinou, Variance reduction in particle methods for solving the Boltzmann equation, in: Proceedings of the Fourth International Conference on Nanochannels, Microchannels and Minichannels, Paper ICNMM2006-96089, 2006.
[6] L.L. Baker, N.G. Hadjiconstantinou. Variance-reduced particle methods for solving the Boltzmann equation, Journal of Computational and Theoretical Nanoscience, in press.
[7] G.A. Bird, Molecular Gas Dynamics and the Direct Simulation of Gas Flows, Clarendon Press, Oxford, 1994.
[8] T.M.M. Homolle. Efficient particle methods for solving the Boltzmann equation, M.S. Thesis, Aeronautics and Astronautics Department, MIT, January 2007.
[9] W. Wagner, A convergence proof for Bird's direct simulation Monte Carlo method for the Boltzmann equation, J. Stat. Phys. 66 (1992) 1011–1044.
[10] N.G. Hadjiconstantinou, A.L. Garcia, M.Z. Bazant, G. He, Statistical error in particle simulations of hydrodynamic phenomena, J. Comput. Phys. 187 (2003) 274–297.
[11] T.M.M. Homolle, N.G. Hadjiconstantinou, Low-variance deviational simulation Monte Carlo, Phys. Fluids 19 (2007) 041701.

[12] H. Grad, Asymptotic theory of the Boltzmann equation II, in: J.A. Laurmann (Ed.), Rarefied Gas Dyn., Academic Press, 1963, pp. 26–59.
[13] L.L. Baker, Efficient numerical methods for solving the Boltzmann equation for small scale flows, PhD Thesis, Mechanical Engineering Department, MIT, May 2007.
[14] Y. Sone, T. Ohwada, K. Aoki, Temperature jump and Knudsen layer in a rarefied gas over a plane wall: Numerical analysis of the linearized Boltzmann equation for hard-sphere molecules, Phys. Fluids 1 (1989) 363–370.
[15] T. Ohwada, Y. Sone, K. Aoki, Numerical analysis of the shear and thermal creep flows of a rarefied gas over a plane wall on the basis of the linearized Boltzmann equation for hard-sphere molecules, Phys. Fluids 1 (1989) 1588–1599.
[16] T. Ohwada, Y. Sone, K. Aoki, Numerical analysis of the Poiseuille and thermal transpiration flows between parallel plates on the basis of the Boltzmann equation for hard-sphere molecules, Phys. Fluids 1 (1989) 2042–2049.
[17] K. Aoki, S. Takata, H. Aikawa, F. Golse, A rarefied gas flow caused by a discontinuous wall temperature, Phys. Fluids 13 (2001) 2645–2661.
[18] Cercignani C. Slow Rarefied Flows: Theory and Application to Micro-Electro-Mechanical Systems, 2006.
[19] N.G. Hadjiconstantinou, The limits of Navier–Stokes theory and kinetic extensions for describing small-scale gaseous hydrodynamics, Phys. Fluids 18 (2006) 111301.
[20] R.E. Denton, M. Kotschenreuther, δf algorithm, J. Comput. Phys. 119 (1995) 283–294.
[21] A.M. Dimits, W.W. Lee, Partially linearized algorithms in gyrokinetic particle simulation, J. Comput. Phys. 107 (1993) 309–323.
[22] B.J. Albright, D.S. Lemons, M.E. Jones, D. Winske, Quiet direct simulation of Eulerian fluids, Phys. Rev. E 65 (2002) 055302R.
[23] W. Peter, Quiet direct simulation Monte-Carlo with random timesteps, J. Comput. Phys. 221 (2007) 1–8.
[24] N.G. Hadjiconstantinou, Sound-wave propagation in transition-regime micro- and nanochannels, Phys. Fluids 14 (2002) 802–809.